Università degli Studi di Bari

PhD course in Physics – XXXIV cycle

Study of the electro-thermal properties and acoustic coupling of quartz tuning forks

Tutors: Prof. Vincenzo Spagnolo, Dott. Pietro Patimisco
PhD candidate: Stefano Dello Russo

Second year PhD report

Introduction

Quartz tuning fork (QTF) is a crystal electro-mechanical oscillator with very unique properties: high resonance quality-factor ($>$ 10000 at atmospheric pressure), small size and insensitivity to ambient acoustic noise as well as their cost-effectiveness. Due to its excellent advantages, starting from 2002 [1], QTFs have been widely used in the field of photoacoustic spectroscopy (PAS), in the so-called Quartz Enhanced PAS (QEPAS). In the last decade, the study of the resonance and acousto-electrical transduction properties of QTFs has led to the design of custom QTFs optimized for QEPAS [2], making the technique well-established and nowadays adopted in many applications, including human health monitoring, environmental protection, industrial process control and geochemistry. Moreover, QTFs have been used as optical detectors in Tunable Diode Laser Absorption Spectroscopy (TDLAS) [3]. This approach, called light induced thermoelastic spectroscopy (LITES), has been recently explored in the last two years. The study of thermoelastic properties has led to the realization of custom QTFs with higher performance of those obtainable by commercially available standard QTFs. Although improvements have been already reported by employing a custom QTF, a detailed study of the influence of thermoelastic properties on the geometrical and resonance properties of the QTF are mandatory to determine guidelines for improve the LITES performance.

In this scenario, during my second year of PhD, a detailed study of the LITES performance with respect to the QTF resonance properties has been performed. In particular, the study has been focused on:

- study of the spatial mapping of LITES signal at different laser spot positions on the QTF prong.
- study of the dependence of the signal-to-noise ratio (SNR) on the QTF strain field intensity and accumulation time, for six different QTFs.
- comparison between QTF and commercial detectors in the near-IR spectral range.
- study of the dependence of the SNR on the pressure of air surrounding the QTF.

Moreover, in July and June 2020, I designed and realized a compact QEPAS sensor for the detection of methane and water vapor in atmosphere. The sensor was calibrated in laboratory by using certified gas concentrations and then it was tested out-of-laboratory, close to a traffic light in the Campus area.

Light-induced thermo-elastic spectroscopy with custom QTFs

When an electromagnetic radiation hits the surface of the QTF, photothermal energy is generated because of light absorption by the quartz. Due to the thermo-elastic conversion, elastic deformations put prongs into vibration if the laser is intensity-modulated at one the QTF resonance frequencies. This effect is enhanced when the radiation is focused close to the prong clamped end, named hereafter prong base, where the stress field is supposed to be mainly located to. To evaluate the performance of different QTFs in LITES, a single-mode continuous wave pigtailed near-IR laser diode (LD), tuned in order to target a water vapor absorption line falling at 1.367 µm, was used as excitation source. The laser beam was coupled with a fiber collimator and aligned through a 50 cm-long absorption cell filled with ambient air containing 1% of water vapor. The light transmitted by the cell was focused on the QTF with a lens having a focal length of 50 mm. A stainless-steel housing, fixed to 5-degree of freedom translation stage, equipped with two near-IR windows was realized in order to accommodate and easily replace the QTFs. The laser current was modulated at half of the QTF resonance frequency while the QTF signal demodulated at the QTF resonance frequency (WMS and 2f detection).

As first step, a mapping of the LITES signal at different laser spot positions on the QTF plane was performed. The investigated QTF (named hereafter as QTF#1) has a prong length of L = 10 mm and width of 0.9 mm, with a crystal thickness of T = 0.25 mm. The QTF is positioned on the plane perpendicular to the laser beam direction. While the laser beam position is fixed, the QTF is translated along x and y axes on the QTF plane. A 2D-map of the LITES signal values at different positions of the laser spot on the QTF plane was obtained. The map of the LITES signal is reported in Fig. 1, for the QTF vibrating at the fundamental mode (Fig. 1(a)) and at the first overtone mode (Fig. 1(c)). The piezoelectric charges generated by prongs vibrations accumulate where the induced strain is maximum. To calculate the strain spatial distribution when the QTF is forced to vibrate at one of its eigenfrequencies modes, a finite element method (FEM) modelling was implemented using COMSOL Multiphysics. The strain distribution in the QTF plane at the fundamental and overtone mode are shown in arbitrary units respectively in Fig. 1(b) and Fig. 1(d).

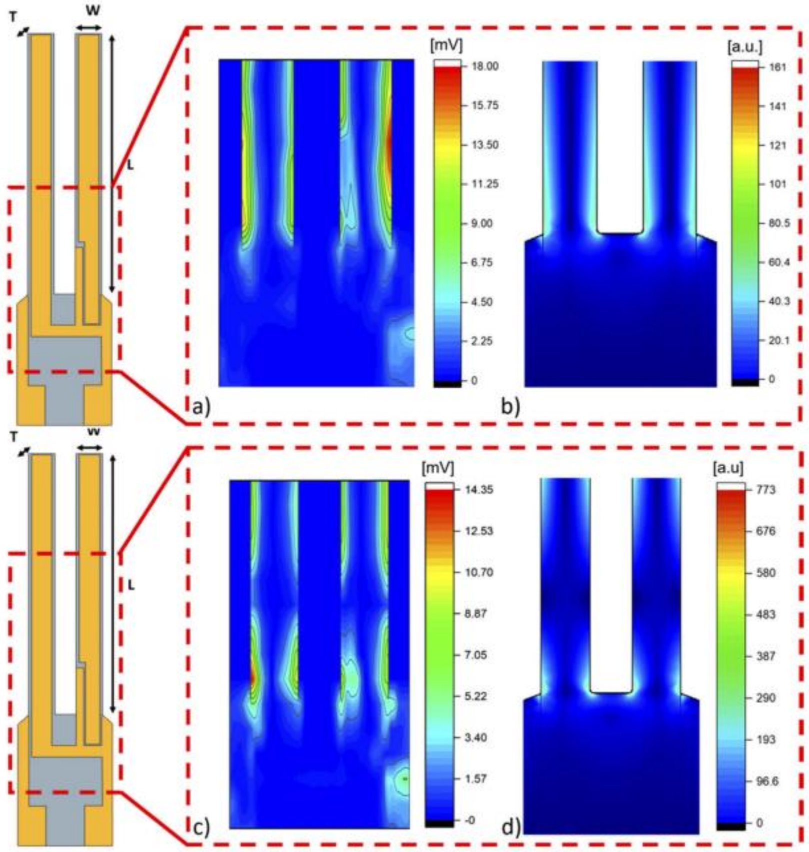

Fig. 1. (a) LITES peak signal mapping and (b) COMSOL simulation of the strain field for QTF#1 fundamental resonance mode. (c) LITES peak signal mapping and (d) COMSOL simulation of the strain field for QTF#1 first resonance overtone mode. LITES signal color scale reports signal intensities in mV while the intensity of the strain field is reported in arbitrary unit. The LITES signal was mapped only on the QTF surface and not outside of it in order to provide a direct comparison with the simulated strain field.

The map of LITES signal peak values retraces the spatial distribution of the strain field: the maximum LITES signal occurs where the strain reaches its highest values. This correlation is also evident when the QTF vibrates at the first resonance overtone: along the prong edge, the lowest LITES signal occurs at nodes point of the strain field (~2 mm far from the prong base), for both QTF prongs. The same investigation was then performed by replacing QTF#1 with a T-shaped QTF (named hereafter as QTF#2). The T-shaped QTF has 50 µm-deep rectangular grooves carved on both prong sides and its geometry is schematized in Fig. 2. The prong has a full length of L = L1 + L2 = 9.4 mm, a crystal thickness of T = 250 µm, and W1 and W2 are 2 mm and 1.4 mm, respectively.

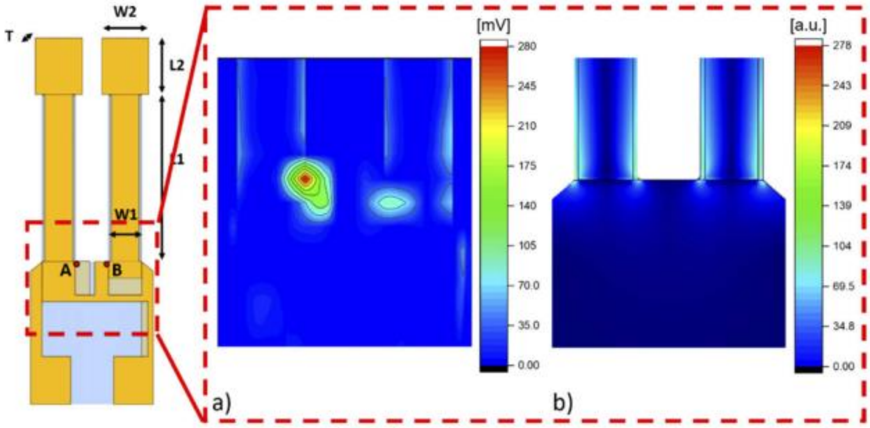

Fig. 2. (a) LITES peak signal mapping and (b) COMSOL simulation of the strain field for QTF#2 fundamental resonance mode. LITES signal color scale reports signal intensities in mV while the intensity of the strain field is reported in arbitrary unit. The points A and B on the QTF schematic in the left side of the figure indicate the positions of the main local maxima of the LITES signal.

As for QTF#1, the spatial distribution of LITES signal shows a good match with the simulated pattern of strain distribution. However, in this case, the highest LITES signal was recorded on the right side of the left prong base (point A in the QTF schematic of Fig. 1). At the specular point B on the left side of the right prong end, the LITES signal is ~4.2 times lower with respect to A. This asymmetry can be ascribed to the gold electrode pattern deposited on the junction area between two prongs. The investigation of the LITES signal on the QTF plane demonstrated its dependence on the strain induced by the prong vibration as well as the influence of the gold layer pattern deposited on the quartz crystal. However, the areas where the maximum strain occurs are not on the QTF plane. An extensive investigation of the LITES signals has been performed as a function of both azimuth and polar angles by shining the area located on the internal side of a prong. With respect to in-plane measurement, for QTF#1 the LITES signal is enhanced by a factor of ~6.3 when the optimal polar angle is selected.

Other four different QTFs were tested in the same LITES setup. In Fig. 3, the achieved LITES SNRs are plotted as a function of the product between the maximum strain ε and the QTF accumulation time τ , at the best operating conditions.

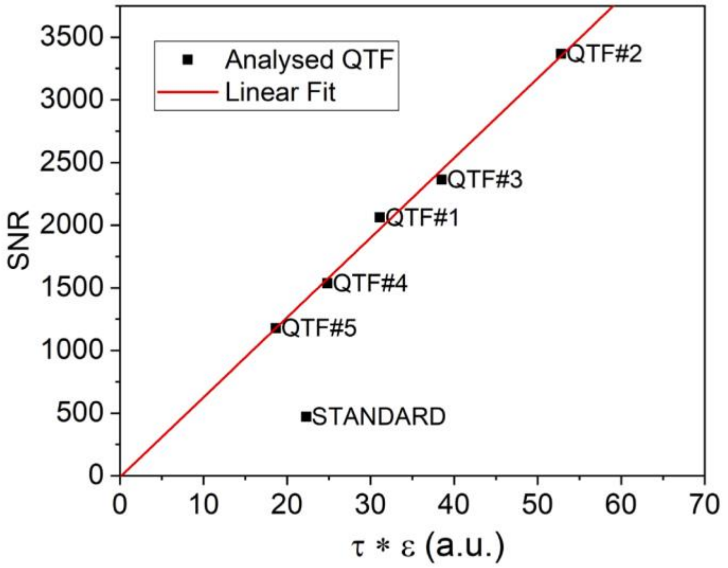

Fig. 3. (Black squares) Calculated SNR as a function the product between accumulation time and strain for all the QTFs analysed. The red line represents the best linear fit.

Apart from standard QTF, LITES SNR values follow a linear trend as a function of the product τ·ε. The reason of the discrepancy observed for the standard QTF is ascribed to the geometrical dimensions of the standard QTF, which is significantly smaller than the other custom QTFs.

The QTF#2 is the one showing the highest SNR and has been selected for a performance comparison with a commercial photodetector. In the LITES setup, with the same experimental conditions, QTF#2 has been replaced by a photodetector (THORLABS PDA10CFEC) operating in the near-IR. The spectral scans of the water absorption line signals recorded with LITES using QTF#2 and acquired with the photodetector are shown in Fig. 4. For an easy comparison, peak values are normalized to the unit for both acquisitions.

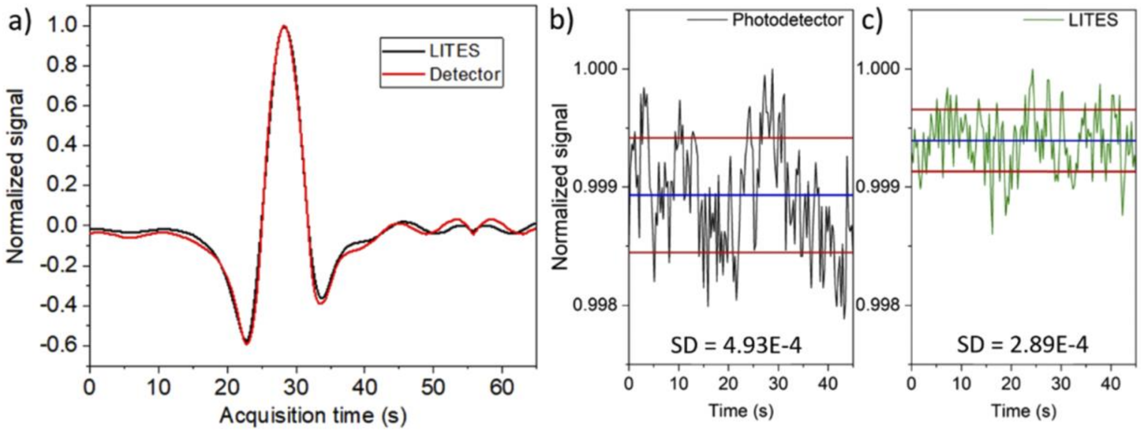

Fig. 4. a) Comparison between normalized QTF#2 LITES signal (black curve) and photodetector signal (red curve). (b) LITES and (c) photodetector signal as a function of time when the laser is locked on the water absorption line. The noise level is extracted as the standard deviation (1σ-value) of the dataset. Being both signals normalized to the unit, the ratio between 1σ-noise levels provides the SNR enhancement of the QTF with respect to the photodetector.

The photodetector SNR was ~2030, 1.65 times lower than that obtained with QTF#2 (SNR of ~3500, see Fig. 3). This indicates that the QTF can provide higher performance for light detection with respect to commercial amplified photodetectors. Exploiting the dependence of the LITES SNR from the QTF accumulation time, if lowering the pressure within the QTF housing, an increase of the QTF quality factor is predicted as well as an increase of the accumulation time. Thereby, an enhancement of the LITES signal is expected. By reducing the pressure from 700 to 5 Torr, the LITES SNR as well as the QTF accumulation time have been measured as a function of the pressure. Since the 1σ-noise level slightly increases as the pressure decreases (when the pressure is reduced from 760 Torr to 5 Torr, the noise level increases only of 10%), the SNR has been selected as figure of merit to describe the QTF performance when used as an optical detector. For an easy comparison, both trends have been reported in the same graph where QTF accumulation time and LITES SNR have been normalized to the values obtained at atmospheric pressure. The results are shown in Fig. 5.

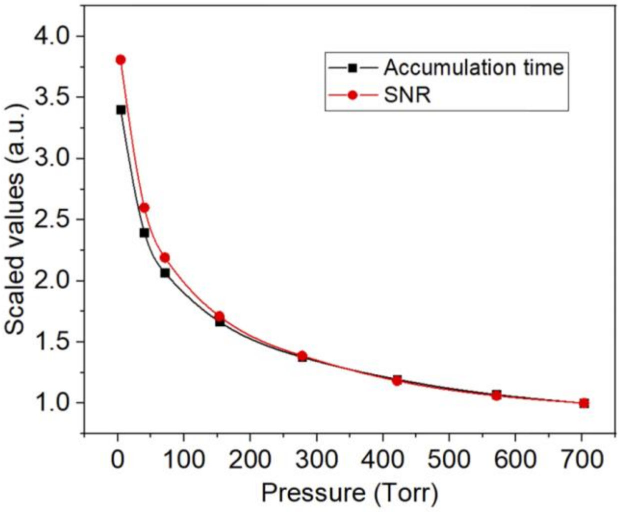

Fig. 5. Scaled values of the LITES SNR (red dots) and accumulation time (black squares). Continuous lines are guide for eye.

As the pressure increases, the LITES SNR follows almost the same trend as the QTF accumulation time, confirming the above assumptions. At 5 Torr, LITES SNR results ~13500, i.e. ~4 times higher than that obtained at atmospheric pressure, and ~6.5 times higher than that measured by using the commercial photodetector.

QTF#2 performances in TDLAS were finally evaluated by using five different types of laser sources, operating in the 1-10.5 µm range. The same set of measurements was repeated by replacing the QTF with four commercially available photodetectors. This study led to a comparison, in terms of minimum detection limit (MDL), between QTF and commercially available detectors. The results are shown in Table 1, together with the laser sources and gas target main features.

Laser type	Wavelength (µm)	Power (mW)	Gas target	Pathlength (cm)	Linestrength (cm/mol)	Detector	MDL (ppm)
LD	1.36	3.5	H_2O	1000*	$8.84\cdot10^{-21}$	QTF PDA10CF-EC	0.74 4.93
LD	1.65	1.13	CH_4	15	$9.27\cdot10^{-22}$	QTF PDA10CF-EC	3.5 2.27
ICL	3.33	1.2	CH_4	60	$4.57\cdot10^{-20}$	QTF PVI-4TE-4	1.98 2.9
QCL	5.26	5.1	H_2O	60	$3.13\cdot10^{-22}$	QTF PVI-4TE-6	14.05 138.5
QCL	10.34	5.6	NH_3	15	$5.19\cdot10^{-19}$	QTF PVI-4TE-10.6	0.28 0.34

Table 1. Minimum detection limits and main features of laser sources and target gases used for LITES and commercial detector TDLAS analysis. *: Multipass cell. LD: Laser Diode, ICL: Interband Cascade Laser, QCL: Quantum Cascade Laser.

Except for the analysis performed with the laser diode and the multipass cell in the Near-IR (Row 2, Table 1), when employed as optical detector in a TDLAS sensor, the QTF performances can be comparable with respect to those obtained for commercial detectors. In conclusion, the QTF can be candidate as excellent detector for the whole spectral range where gas molecules roto-vibrational transitions fall.

CH_4 and H_2O concentration measurements near a traffic light

Methane (CH_4) is one of the main anthropogenic greenhouse gases in the atmosphere. Its concentration has increased up to 1.87 ppm, starting from a value of 715 ppb in preindustrial times. Due to the effect of CH_4 on global warming and climate change, methane detection is mandatory to monitor variations in atmospheric concentration as well as identify its main sources. These objectives can be fulfilled by real-time and in situ measurements of CH_4 concentration in the atmosphere. Thus, a methane sensor must guarantee the following: (i) high sensitivity in the sub-part-per-million range; (ii) high selectivity to discriminate the CH4 signal from other gas components in the atmosphere; and (iii) fast response time to track any variation in concentration. Moreover, robustness, compactness, and insensibility to environmental external noise are required for in-field operation. For QEPAS sensing, the generation of the acoustic wave, and consequently of the QEPAS signal, depends on the relaxation rate of the excited molecules' vibrational energy into the kinetic energy (translation) of the surrounding molecules (V-T relaxation). Several works demonstrated the linear increment of the CH_4 photoacoustic signal with the water content, when the CH_4 concentration is below 1%. For these reasons a compact QEPAS sensor, that is able to evaluate concentrations of methane and water vapor in a sequential way, has been realized.

The compact QEPAS sensor-head, consisting of laser source and acoustic detection module (ADM), is shown in Fig. 6. The light source was a laser diode emitting at 1.65 µm, capable of targeting two nearby CH_4 and H_2O absorption lines in the whole current dynamic range. The laser beam was collimated and sent into the ADM. The ADM contained a custom quartz tuning fork with fundamental resonance frequency f_0 = 12463.9 Hz at 760 Torr. The QTF was acoustically coupled with two 12.4 mm long tubes with internal diameter of 1.6 mm to amplify the acoustic wave and enhance the QEPAS signal. QEPAS measurements were performed using wavelength modulation with 2f-detection: a sinusoidal modulation was applied to the laser current at half of the QTF resonance frequency, and the QTF response was detected at f_0 using a digital lock-in amplifier.

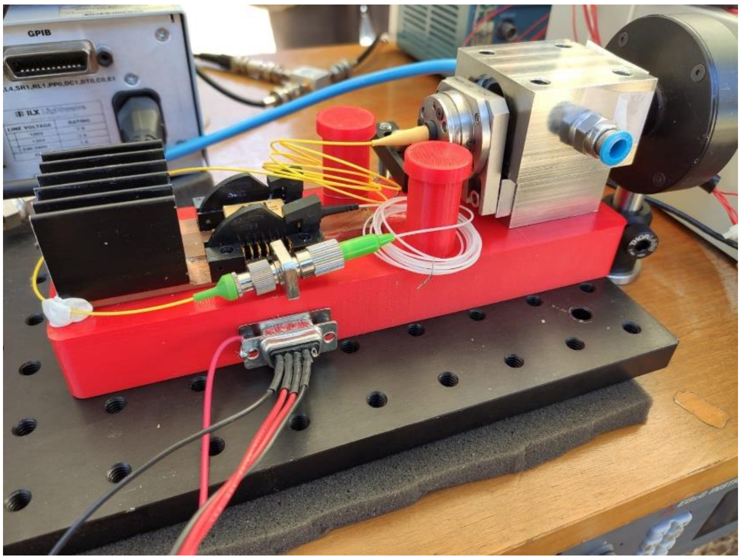

Fig 6. Sensor head, consisting of laser source and acoustic detection module (ADM), used for CH_4 and H_2O concentration measurement near a traffic light

A preliminary calibration of the QEPAS sensor for the detection of CH_4 in dry N_2 was performed. The QEPAS peak signal was measured as a function of the gas pressure. The optimal gas pressure that maximizes the QEPAS signal was 500 Torr. Then, the QEPAS peak signal was measured at different concentrations of methane at the optimal pressure. The mixtures were obtained starting from a certified concentration of 500 ppm of CH_4, which was diluted in pure N_2 by means of a gas mixer. The results of the calibration analysis are shown in Fig. 7.

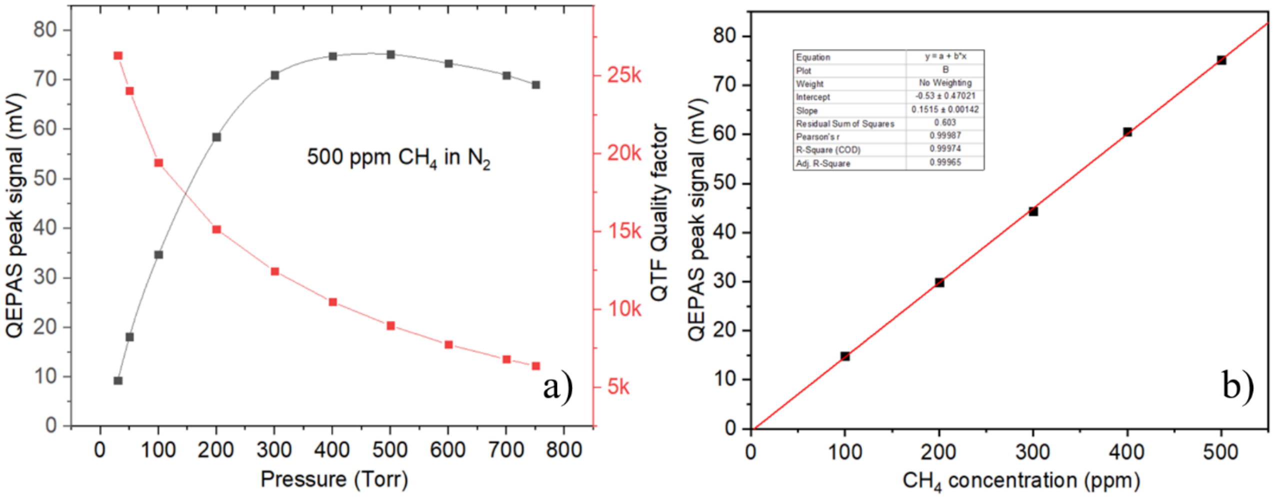

Equation	y = a + b*x
Plot	B
Weight	No Weighting
Intercept	-0.53 ± 0.47021
Slope	0.1515 ± 0.00142
Residual Sum of Squares	0.603
Pearson's r	0.99987
R-Square (COD)	0.99974
Adj. R-Square	0.99965

Fig 7. QEPAS sensor calibration for methane. a) QEPAS peak signal and QTF quality factor pressure behavior. b) QEPAS CH4 linear response, at a pressure of 500 Torr, in the range 100 - 500 ppm

The calibration curve y = (152 µV/ppm) · x was obtained with an $R^2 = 0.999$ by a linear fit of the experimental data in Fig. 7b. A minimum detection limit of ~600 ppb was achieved with a 1σ noise of 91 µV, at 2 s integration time. The minimum detection limit is lower than the standard concentration of methane in atmosphere. However, the analysis of methane concentration in a specific environment requires the study of the influence of water vapor on the CH_4 QEPAS peak signal. Therefore, a PermSelect membrane was used to modify and stabilize the water concentration within the sensor head. With a water concentration varying in the range 1 – 4 % at a pressure of 500 Torr, the CH_4 QEPAS peak value was almost unchanged, when the CH_4 concentration is fixed. A LabVIEW software was developed to automatize the acquisition and store the data. Finally, the QEPAS sensor-head was installed close to a traffic light, within the campus area (coordinates 41°06'27.9"N 16°53'06.3"E). The measurements were performed in a time span of 22 hours, from 19:00 of 29th July 2020 to 17:00 of 30th July 2020, with an averaged 0 km/h wind and 0 mm precipitation conditions, at a temperature ranging from 23 °C to 32 °C. The water vapor concentration values were compared with those calculable starting from relative humidity (RH) and temperature provided by a weather station located less than 3 km far from the sensor head location (http://my.meteonetwork.it/station/pgl148/). All the results obtained are shown in the Fig. 8. The raw data were averaged with a moving average of 30 points, equivalent to a signal average of 15 minutes.

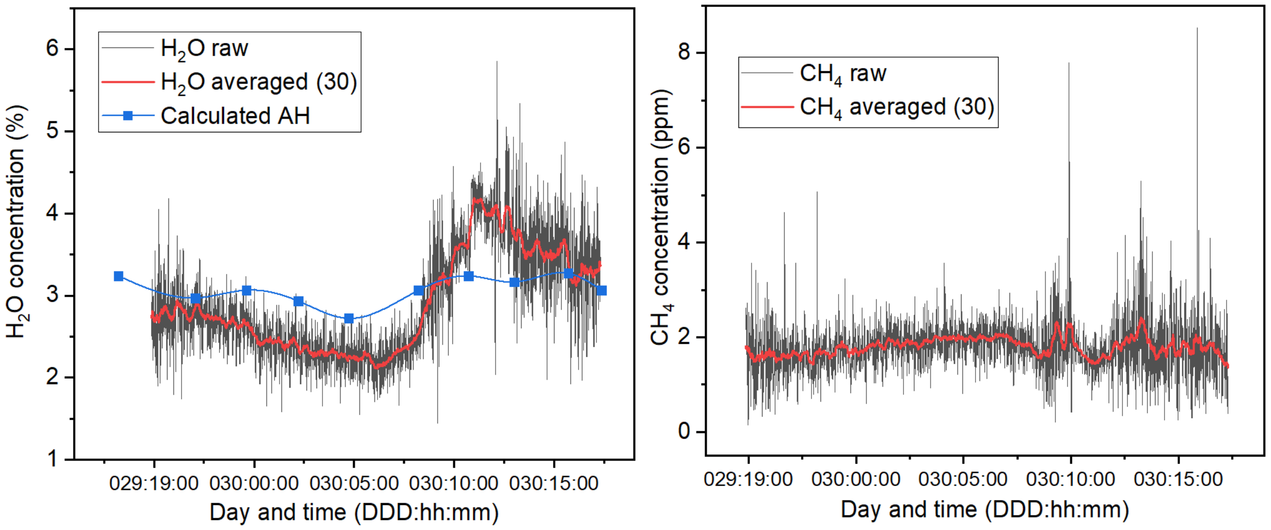

Fig 8. 22 hours QEPAS CH_4 and H_2O measurement near a traffic light in Bari city. Black line: raw data. Red line: 30 points averaged data. Blue line: calculated Absolute Humidity (AH) from data provided by a weather station nearby.

A good agreement was found with values measured by the QEPAS sensor-head and those calculated from the measurements provided by the weather station. It is worth noticing that the water vapor concentration is highly influenced by human activities as well as by the territory morphology in the immediate proximity. The average value of the methane concentration during the night period is equal to 1.8 ppm, in excellent agreement with the values recently reported in the literature. During the daytime hours, and in particular during rush hours, the methane concentration increases and reaches peak values up to 8.5 ppm. In addition, average values of 2.4 ppm were measured during two rush periods, one starting around at 10:00 am and the other one starting at 2:00 pm. Thus, these results could be highly correlated to car emissions. However, the analysis of the reported data is still ongoing.

References

[1] A.A. Kosterev, Y.A. Bakhirkin, R.F. Curl, F.K. Tittel, “Quartz-enhanced photoacoustic spectroscopy”, Optics Letters, 27(21), 1902-1904 (2002).

[2] P. Patimisco, A. Sampaolo, L. Dong, F.K. Tittel, V. Spagnolo, “Recent advances in quartz enhanced photoacoustic sensing”, App. Phys. Rev. 5, 011106 (2018).

[3] Y. Ma, Y. He, Y. Tong, X. Yu, F. K. Tittel, “Quartz-tuning-fork enhanced photothermal spectroscopy for ultra-high sensitive trace gas detection”, Opt. Express 26(24), 32103–32110 (2018).

List of attended courses

- Promozione della ricerca scientifica (Prof. De Gennaro)
- How to prepare a technical speech in English (Prof. White)
- Programming with Python for Data Science (Prof. Diacono)
- Atom-photon interactions (Prof. Pepe)
- Optical sensors and spectroscopic techniques (Prof. Patimisco)
- Applications of MATLAB (Prof. Dotoli)
- Introduction to C++ programming (Prof. Cafagna)

List of publications

1. **S. Dello Russo**, S. Zhou, A. Zifarelli, P. Patimisco, A. Sampaolo, M. Giglio, D. Iannuzzi, V. Spagnolo, “Photoacoustic spectroscopy for gas sensing: a comparison between piezoelectric and interferometric readout in custom quartz tuning forks”, Photoacoustics **2020**, 17, 100155.

2. F. Sgobba, G. Menduni, **S. Dello Russo**, A. Sampaolo, P. Patimisco, M. Giglio, E. Ranieri, V. M. N. Passaro, F. K. Tittel, V. Spagnolo, “Quartz-Enhanced Photoacoustic Detection of Ethane in the Near-IR Exploiting a Highly Performant Spectrophone”, Appl. Sci. **2020**, 10(7), 2447.
3. G. Menduni, A. Sampaolo, P. Patimisco, M. Giglio, **S. Dello Russo**, A. Zifarelli, A. Elefante, P.Z. Wieczorek, T. Starecki, V.M.N. Passaro, F.K. Tittel, V. Spagnolo, “Front-End Amplifiers for Tuning Forks in Quartz Enhanced PhotoAcoustic Spectroscopy”, Appl. Sci. **2020**, 10(8), 2947.
4. **S. Dello Russo**, A. Zifarelli, P. Patimisco, A. Sampaolo, T. Wei, H. Wu, L. Dong, V. Spagnolo, “Light-induced thermo-elastic effect in quartz tuning forks exploited as a photodetector in gas absorption spectroscopy”, Optics Express **2020**, 28, 19074.
5. B. Sun, A. Zifarelli, H. Wu, **S. Dello Russo**, S. Li, P. Patimisco, L. Dong and V. Spagnolo, “Mid-infrared quartz-enhanced photoacoustic sensor for ppb-level CO detection in SF6 gas matrix exploiting a T-grooved quartz tuning fork”, Analytical Chemistry **2020**, 92, 13922-13929.

Conference proceedings

1. **S. Dello Russo**, P. Patimisco, A. Sampaolo, M. Giglio, G. Menduni, A. Elefante, V.M.N. Passaro, F.K. Tittel, V. Spagnolo, “Measurement of non-radiative gas molecules relaxation rates by using quartz-enhanced photoacoustic spectroscopy”, Proc. SPIE, Quantum Sensing and Nano Electronics and Photonics XVII, **2020**.
2. P. Patimisco, S. Zhou, **S. Dello Russo**, A. Zifarelli, A. Sampaolo, M. Giglio, H. Rossmadl, V. Mackowiak, A. Cable, D. Iannuzzi, V. Spagnolo, “Comparison between interferometric and piezoelectric readout of tuning fork vibrations in quartz-enhanced photoacoustic spectroscopy”, Proc. SPIE, Quantum Sensing and Nano Electronics and Photonics XVII, **2020**.